

SAR Exploration of Tight Binding Inhibitors of Influenza Virus PA Endonuclease

Cy V. Credille, Christine N. Morrison, Ryjul Wynn Stokes, Benjamin
Dick, Yifan Feng, Jiaxing Sun, Yao Chen, and Seth M. Cohen

J. Med. Chem., **Just Accepted Manuscript** • DOI: 10.1021/acs.jmedchem.9b00747 • Publication Date (Web): 19 Sep 2019

Downloaded from pubs.acs.org on September 20, 2019

Just Accepted

"Just Accepted" manuscripts have been peer-reviewed and accepted for publication. They are posted online prior to technical editing, formatting for publication and author proofing. The American Chemical Society provides "Just Accepted" as a service to the research community to expedite the dissemination of scientific material as soon as possible after acceptance. "Just Accepted" manuscripts appear in full in PDF format accompanied by an HTML abstract. "Just Accepted" manuscripts have been fully peer reviewed, but should not be considered the official version of record. They are citable by the Digital Object Identifier (DOI®). "Just Accepted" is an optional service offered to authors. Therefore, the "Just Accepted" Web site may not include all articles that will be published in the journal. After a manuscript is technically edited and formatted, it will be removed from the "Just Accepted" Web site and published as an ASAP article. Note that technical editing may introduce minor changes to the manuscript text and/or graphics which could affect content, and all legal disclaimers and ethical guidelines that apply to the journal pertain. ACS cannot be held responsible for errors or consequences arising from the use of information contained in these "Just Accepted" manuscripts.

SAR Exploration of Tight Binding Inhibitors of Influenza Virus PA Endonuclease

Cy V. Credille,^{1†} Christine N. Morrison,^{1†} Ryjul W. Stokes,^{1†} Benjamin Dick,^{1‡} Yifan Feng,^{2‡} Jiaying Sun,² and Yao Chen,^{2,*} and Seth M. Cohen^{1,3,*}

¹Department of Chemistry and Biochemistry, University of California, San Diego, La Jolla, CA 92093, United States

²State Key Laboratory of Medicinal Chemical biology, Nankai University, No.94 Weijin Road, Nankai District, Tianjin, P.R.China 300071

³Lead corresponding author [†]Authors contributed equally [‡]Authors contributed equally

Supporting Information Placeholder

ABSTRACT: Significant efforts have been reported on the development of influenza antivirals including inhibitors of the RNA-dependent RNA polymerase PA N-terminal (PA_N) endonuclease. Based on recently identified, highly active metal-binding pharmacophores (MBPs) for PA_N endonuclease inhibition, a fragment-based drug development (FBDD) campaign was pursued. Guided by coordination chemistry and structure-based drug design (SBDD), MBP scaffolds were elaborated to improve activity and selectivity. Structure-activity relationships (SARs) were established and used to generate inhibitors of influenza endonuclease with tight binding affinities. The activity of these inhibitors was analyzed using a fluorescence quenching-based nuclease activity assay and binding was validated using differential scanning fluorimetry (DSF). Lead compounds were found to be highly selective for PA_N endonuclease against several related dinuclear and mononuclear metalloenzymes. Combining principles of bioinorganic and medicinal chemistry in this study has resulted in some of the most active in vitro influenza PA_N endonuclease inhibitors with high ligand efficiencies.

INTRODUCTION

Annual influenza epidemics are responsible for substantial morbidity and mortality, as well as significant financial burden worldwide. Vaccinations against the influenza virus are generally effective for healthy individuals, but they must be re-administered annually and are less effective for the elderly, immunocompromised, or other high-risk individuals. Vaccine efficacy is also dependent on correctly predicting the major type among circulating viral strains each season, and incorrect predictions of the principal infectious strain have rendered previous vaccines <30% effective (e.g., during the 2017-2018 flu season).^{1,2} Rapid mutation and antigenic variation, due to genetic reassortment, drive both the emergence of novel pandemic strains of the influenza virus as well as the appearance of antiviral resistance to existing treatments.^{3,4} Although antiviral drugs have been developed, the number of antivirals that can be used for prophylaxis and therapeutic treatment of severe influenza infection is limited.⁵ Three classes of small molecule treatments for influenza have been approved by the U.S. Food and Drug Administration (FDA). Two of these are M2 ion-channel blockers and neuraminidase inhibitors. However, viral resistance to existing inhibitors and the time-dependent effectiveness of neuraminidase inhibitors persist as major challenges to current approved therapies.⁶⁻¹⁰ Considering this, there is an urgent need for the development of new drugs to prevent and treat influenza infection. The N-terminal PA endonuclease component of the RNA-dependent RNA polymerase (PA_N) is an attractive target to meet this need. The PA_N endonuclease inhibitor baloxavir¹¹ (Figure 1) was recently approved for use in the U.S.

All influenza viruses contain a segmented single-stranded negative sense RNA genome.¹² Each RNA segment is packaged in complex with a single heterotrimeric RNA-dependent RNA

polymerase complex comprised of three distinct proteins (PA, PB1, PB2).^{13,14} Following viral infection, the viral polymerase-RNA complex is transported to the host cell nucleus where the polymerase complex catalyzes both transcription and replication of the viral genome.¹⁵ However, the polymerase complex is unable to incorporate or synthesize the 5'-mRNA cap necessary for eukaryotic translation.^{16,17} To overcome this limitation, the PB2 protein captures a capped mRNA or pre-mRNA by tightly binding to the 5'-cap structure. The host mRNA is then cleaved 8-14 nucleotides downstream from the cap by the viral PA (or P3 in the case of Influenza C) endonuclease domain.¹⁷⁻¹⁹ The sequestered, capped RNA segment then serves as a primer for viral RNA synthesis by the PB1 protein of the polymerase complex. This 'cap-snatching' mechanism enables formation of the viral mRNAs which are translated to viral proteins by the host cell machinery.

The viral RNA polymerase is a validated target for the development of new antiviral therapies. Of particular interest is the PA endonuclease domain of influenza A and B viruses. The PA endonuclease domain lacks a human homologue and is highly conserved among all circulating influenza strains, including pandemic and avian strains.³ The PA subunit can be divided into two domains connected by a long flexible peptide chain: the C-terminal domain, which is primarily structural in nature, and the N-terminal domain which contains the endonuclease catalytic site. The N-terminal domain of the PA (PA_N) endonuclease is a dinuclear metalloenzyme that can bind to either Mg²⁺ or Mn²⁺ cations, but shows a preference for Mn²⁺ in both metal ion affinity and catalytic activity.^{17,20} The metal cations are coordinated by five active site residues (His41, Ile120, Asp108, Glu80, Glu119) and several water molecules, forming a dinuclear complex that is bridged by Asp108 and a catalytically active water/hydroxide anion in the native structure (Figure 1).^{17,21}

Previous studies have identified highly active metal-binding pharmacophore (MBP) fragments for the PA_N endonuclease metal

site, including compound **1** which is reported to inhibit PA_N endonuclease activity with an IC_{50} value of 17 nM (Figure 1).²² Related fragments, such as 2-substituted-4,5-dihydropyrimidines, have been identified from campaigns that employed a novel fluorescence polarization assay.²³ Herein, a fragment-based drug discovery (FBDD) campaign was initiated based on compound **1**. Several of these leads were elaborated and optimized, resulting in compounds that possess in vitro inhibitory activity with IC_{50} values of <1 nM against PA_N endonuclease in fluorescence quenching-based nuclease activity assays. These are among the most active in vitro inhibitors of this enzyme reported to date and show high ligand efficiencies.

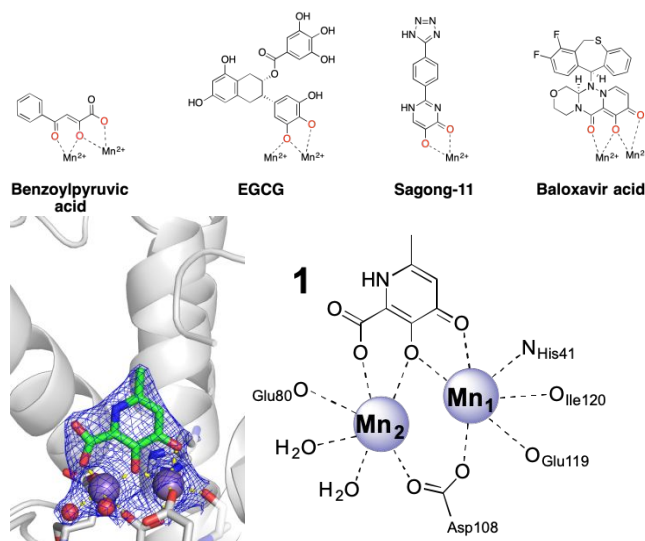


Figure 1. *Top:* Structures of several reported metal-binding inhibitors of PA_N endonuclease.^{24,25} *Bottom Left:* Structure of the dinuclear metal active site of PA_N endonuclease with the active site metal centers coordinated by compound **1** (IC_{50} = 17 nM),²² a highly active MBP fragment (PDB 6E6V). The two Mn^{2+} cations are coordinated by three acidic residues (Glu80, Asp108, Glu119), the imidazole nitrogen of His41, and the carbonyl oxygen of Ile120, as a bridged coordination complex. Coordinating waters are shown as red spheres, and coordination bonds are shown as dashed yellow lines. *Bottom Right:* Illustration of the active site metal centers coordinated to compound **1**. The three coordinating oxygen atoms from the MBP replace the axial and bridging water/hydroxide molecules that coordinate to the metal centers in the native protein.

To confirm the high binding affinity of these compounds, differential scanning fluorimetry (DSF) assays were used to identify the change in melting temperature (ΔT_M) between inhibitor-free and inhibitor-bound PA_N endonuclease. A strong linear correlation was observed between inhibitory activity (pIC_{50}) and ΔT_M across multiple inhibitor chemotypes. Using this relationship, the pIC_{50} values of compounds with common chemical features were extrapolated to estimate values that were otherwise below the detection limit of the fluorescence quenching-based nuclease activity assay. X-ray crystallography studies of these inhibitors bound to PA_N endonuclease show key interactions with active site residues, including Lys34, Arg124, and a small pocket near Ile38. Several of these lead molecules were assayed against H1N1 influenza A in cell-based viral neutralization studies. The most active compound (**23**) displayed an IC_{50} value of 47 pM, and several inhibitors were found to have EC_{50} values ranging from ~8–21 μM with no mammalian cellular toxicity up to 800 μM , suggesting a wide therapeutic index for their use.

RESULTS AND DISCUSSION

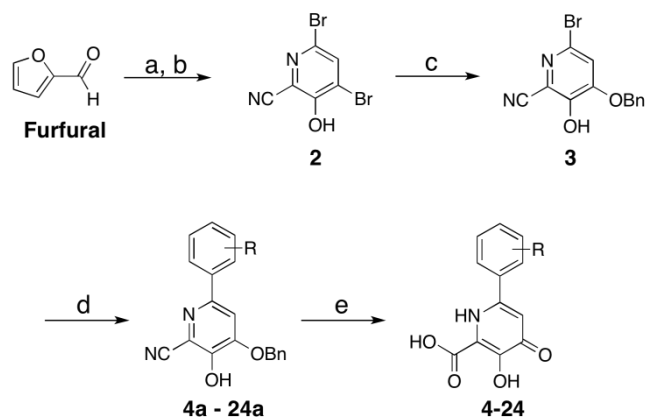
2

Compound **1**, which was previously identified as having excellent metal coordination to the PA_N endonuclease active site,²² was chosen for further hit-to-lead development. To help guide initial structure-activity relationship (SAR) analysis, existing inhibitors were examined that share similar metal-binding motifs with compound **1** (Figure 1), including hydroxypyrimidinones, hydroxypyridinones, β -keto acids, dihydroxybenzoic acids, and catechol derivatives.^{24,25} Prior SAR studies on compound **1** suggested that the 6-position (methyl group) was preferred for further derivatization.²² Elaboration of compound **1** at other ring positions resulted in poorer activity.

Comparing known inhibitors with compound **1**, an aryl-halide cross-coupling strategy for further elaboration was deemed most viable. To generate the desired aryl-halide intermediate in sufficient quantities, an efficient and scalable synthetic route was developed beginning from commercially available furfural (Scheme 1). Generation of the dibromo-hydroxypyridonitrile intermediate **2** is typically performed over five discrete steps but was optimized into a one-pot reaction in >50% overall yield. This advanced intermediate was then selectively functionalized at the 4-position with an activated alcohol to generate compound **3**. This protected species was found to be compatible with Suzuki and Sonogashira cross-coupling reactions; however, Buchwald-Hartwig amination on **3** was unsuccessful. Acid-catalyzed deprotection of the protected intermediates (**4a–24a**, Scheme 1) generated the desired 2-carboxy-3,4-hydroxypyridinone derivatives (**4–24**, Scheme 1).

Using the aforementioned synthetic strategies, a small library of functionalized derivatives of **1** were prepared (Table 1). The compounds were evaluated using an established fluorescence quenching-based nuclease assay.^{26,27} To calibrate our assay, four known PA_N endonuclease inhibitors with a wide range of reported IC_{50} values were used as positive controls (Table S2). The four control compounds were: epigallocatechin gallate (EGCG),²⁸ L-742,001,²⁹ Baloxavir acid (the active form of FDA-approved Baloxavir marboxil),³⁰ and 2,4-dioxo-4-phenylbutanoic acid (DPBA).²⁹ The IC_{50} values for these control compounds, as measured in our laboratory, tended to be ~5- to 10-fold more active than reported values.^{28–30}

The addition of a phenyl ring at the 6-position of the core MBP scaffold (**4**) was well tolerated and resulted in a 3-fold increase in activity versus **1** in fluorescence quenching-based nuclease assays (see ESI for details), which is consistent with previously reported SAR.^{26,27} Addition of a methyl group showed that derivatization was tolerated at the 2'-, 3'-, and 4'-positions (**5–7**), with the 2'-methyl substituent yielding a dramatic increase in inhibition activity below the detection limit of the assay (IC_{50} values of <2 nM at 5 nM enzyme concentration). This SAR trend was validated with bulkier substituents on the phenyl ring, as illustrated by isopropyl (**8–9**) and phenyl ether derivatives (**10–12**) (Table 1).

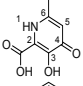
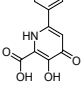
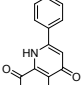


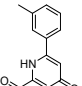
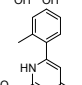
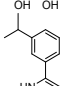
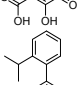
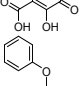
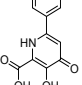
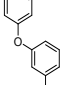
Scheme 1. Synthesis of PA_N endonuclease inhibitors. Reagents and conditions: (a) NH₄OAc, KCN, EtOAc:water, r.t., 18 h; (b) Br₂, HBr, 5 °C 30 min, r.t., 18 h; (c) BnOH, NaH, DMSO, 60 °C, 18-24 h; (d) K₂CO₃, PdCl₂(dppf), SPhos, boronic acid, dioxanes:water, 95 °C, 18 h; (e) HCl, HOAc, TFA, neat, 95 °C, 18 h.

An extensive screen of 2'-substituents revealed that small alkyl substituents are most active, with 2'-methyl, -ethyl, and -trifluoromethyl derivatives (**7**, **13**, **14**) all resulting in IC₅₀ values of <2 nM, which is the detection limit of the in vitro nuclease assay (at an enzyme concentration of 5 nM, Table 2). As the size or hydrophilicity of the 2'-substituents increased, the compounds became less active; for example, isopropyl and phenyl ether derivatives **8** and **12** were found to be less active than smaller methyl, ethyl, and methyl ether derivatives **7**, **13**, and **15**. However, many different functional groups were tolerated, indicating that 2'-substituents were potentially suitable for late-stage chemical modification for adsorption, distribution, metabolism, excretion, and toxicity (ADMET) liabilities. Based on SAR found in other PA_N endonuclease inhibitors that show that polar and acidic 4'-substituents can make favorable contacts with basic active site residues, derivatives of **4** with carboxylic acid or tetrazole groups at either the 3'- or 4'-positions were synthesized. All four derivatives tested (**17**, **18**, **19**, **20**, Table 2) show increased activity relative to **4**, with activity at or below the detection limit of the assay (IC₅₀ values of <2 nM at 5 nM enzyme concentration).

In an effort to maximize the activity of these inhibitors and based on the assumption that the favorable 2'-alkyl and 4'-acidic interactions were not mutually exclusive, a fragment merging strategy was pursued. As shown in Table 3, derivatives were synthesized combining a 2'-methyl group with a 4'-carboxylic acid (**21**), 4'-tetrazole (**22**), or 4'-oxadiazolone (**24**) group. Gratifyingly, these inhibitors displayed IC₅₀ values of <2 nM, indicating that merged inhibitors were as least as active as parent compounds **7**, **17**, and **19**, and that the two functional groups were likely having an additive effect on inhibitor activity. However, these derivatives were too active to generate reliable inhibition data using the nuclease activity assay, despite efforts to further optimize the assay (i.e., the IC₅₀ values were below the minimum usable concentration of enzyme employed in the assay). This lower limit of detection is also shared by other previously reported assays used to determine PA_N endonuclease inhibitor binding, which precluded their use as orthogonal activity assays.³¹ Based on this, alternative biophysical methods were sought to generate binding data for these tight-binding compounds. Toward this goal, differential scanning fluorometry (DSF) was employed as an orthogonal evaluation of inhibitor binding.³²⁻³⁵ This method is more time- and cost-effective than other techniques used to assess ligand binding and can be used for both weak and strong binders.³⁴

Table 1. Activity and binding affinities of derivatives of compound **1**.

Number	Compound	IC ₅₀ (nM)	pIC ₅₀	ΔT _M (°C)
1		17 ± 3	7.8	11.1
4		5.6 ± 1.2	8.3	8.5
5		7.2 ± 2.1	8.1	10.3

6		4.8 ± 1.3	8.3	10.7
7		<2.0	>8.7	13.2
8		6.3 ± 1.8	8.2	10.1
9		3.2 ± 1.1	8.5	11.6
10		25 ± 6	7.6	8.1
11		14 ± 3	7.9	9.0
12		6.0 ± 1.6	8.2	10.4

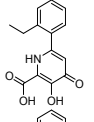
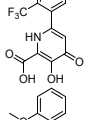
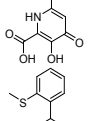
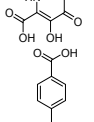
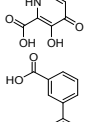
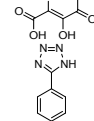
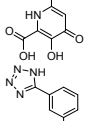
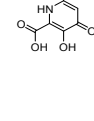
Differential Scanning Fluorometry (DSF). Changes in melting values (ΔT_M) in DSF experiments are proportional to both ligand concentration and ligand binding affinities.^{32,34} The thermal stability of a protein generally increases with favorable protein-ligand contacts made over the total interaction surface of the protein, with tighter-binding interactions (lower K_D) typically resulting in larger increases to the observed melting temperature compared to the native protein.^{32,34} DSF as an inhibitor screening method has been successfully demonstrated with other metalloenzymes such as human carbonic anhydrase I and II (hCAI/hCAII) with sulfonamide-based inhibitors.³⁴ We determined the ΔT_M values of L-742,001, Baloxavir acid, and DPBA (Table S2); the values for Baloxavir acid and DPBA^{29,30} matched reported values well (no prior ΔT_M value for L-742,001 is available).

DSF analysis of compounds **4-20** (Table 1, Table 2) validates the relative binding affinities of these inhibitors and gives insight into compounds that are too active to properly rank-order using the fluorescence quenching-based nuclease assay. Comparing ΔT_M (from DSF) and pIC₅₀ values (from the nuclease assay) for compounds **4-20** results in a linear correlation ($r = 0.98$, $n = 12$, $p < 2 \times 10^{-8}$) for all compounds with activity above the detection limit of the nuclease assay (Figure 2, **4-20**, labeled as 'series A'). To evaluate the robustness of this correlation across chemotypes, the ΔT_M and pIC₅₀ values of two additional, chemically distinct series of inhibitors were compared (Figure S1). One series of compounds (labeled 'series B' in Figure 2) is comprised of previously reported PA_N endonuclease inhibitors bearing a functionalized 3,4-hydroxypyridinone MBP core (Figure S1).²⁷ Compounds in series B coordinate to the active site metal ions in PA_N endonuclease and make a variety of protein contacts, many of which are predicted to be similar to those made by compounds **4-20**. Series B also gave a linear correlation ($r = 0.99$, $n = 8$, $p < 8 \times 10^{-7}$) between ΔT_M and a

wide range of pIC_{50} values. A third grouping of compounds, ('series C', Figure S1) is comprised of various, non-elaborated MBP fragments.²² These molecules coordinate to both active site metal ions but make few other interactions with the remainder of the protein active site. Interestingly, this series also shows a strong linear correlation ($r = 0.995$, $n = 9$, $p < 3 \times 10^{-8}$) between ΔT_M and pIC_{50} values despite gaining most of their binding affinity from metal coordination. Taken together, the DSF evaluation of compounds in series A, B, and C (Figure S1) indicate that qualitative inhibition data can be gained from extrapolation of interrelated ΔT_M and pIC_{50} data for PA_N endonuclease inhibitors with similar chemotypes.

Using the observed linear relationship between DSF ΔT_M measurements and nuclease assay pIC_{50} values, we assigned estimated IC_{50} values for tight binding compounds from series A, as shown in Table 3 and Figure 2 (green diamonds). Based on DSF extrapolation, 2'-methyl, -ethyl, and -trifluoromethyl derivatives (**7**, **13**, **14**), were found to be nearly equipotent with IC_{50} values of ~ 1 nM. Compound **19**, which contains a 4'-tetrazole moiety, was found to be approximately twice as active as the equivalent carboxylic acid-containing analogue **17**, which is consistent with literature reports.^{27,36} Merging 2'-methyl or trifluoromethyl and 4'-acidic moieties (**21**-**24**) resulted in further improvements in activity, with **22** and **23** displaying estimated IC_{50} values of ~ 110 pM and ~ 47 pM, respectively.

Table 2. Activity and binding affinities of derivatives of compound **4**.

Number	Compound	IC_{50} (nM)	pIC_{50}	ΔT_M ($^{\circ}C$)
13		<2.0	>8.7	13.1
14		<2.0	>8.7	13.3
15		2.3 ± 0.6	8.6	11.9
16		3.2 ± 0.5	8.5	11.8
17		<2.0	>8.7	11.9
18		2.3 ± 0.4	8.6	11.7
19		<2.0	>8.7	14.1
20		<2.0	>8.7	12.9

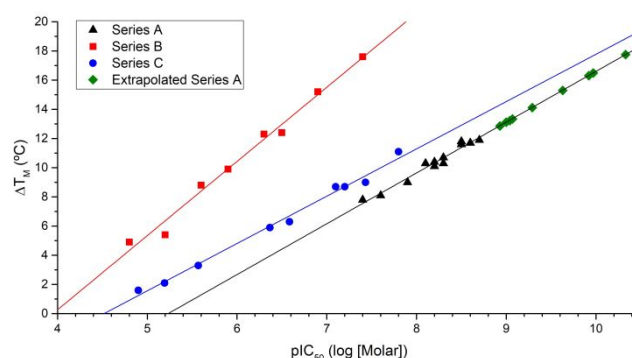
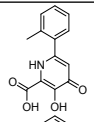
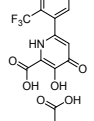
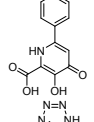
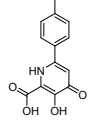
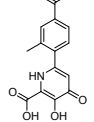
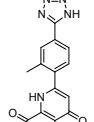
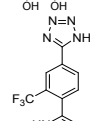
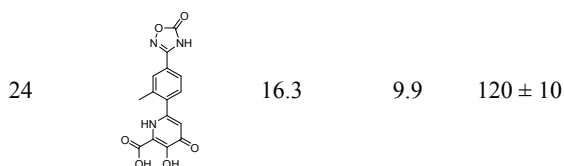


Figure 2. pIC_{50} values for three chemically distinct series of PA_N endonuclease inhibitors are plotted versus ΔT_M measurements obtained by DSF. The data show linear correlations within each chemical series. In series A (**4**-**20**), inhibition values corresponding to green diamonds are extrapolated from experimental ΔT_M values (shown as black triangles; see Tables 2, 3). This analysis allows for estimation of inhibition for compounds with activity below the detection limit of the nuclease assay. Chemical structures of compounds in series B and C are provided in Figure S1, and a version of this figure with all compounds labeled on the plot is provided in Figure S2.

Table 3. Activity and binding affinities of PA_N endonuclease inhibitors derived from ΔT_M values. IC_{50} values listed are estimated from ΔT_M values (see Figure 2).

Number	Compound	ΔT_M ($^{\circ}C$)	pIC_{50}	Estimated IC_{50} (pM)
7		13.2	9.0	920 ± 70
14		13.3	9.1	860 ± 70
17		12.9	8.9	1180 ± 90
19		14.1	9.3	510 ± 40
21		15.3	9.6	230 ± 20
22		16.5	10.0	110 ± 10
23		17.8	10.3	47 ± 6

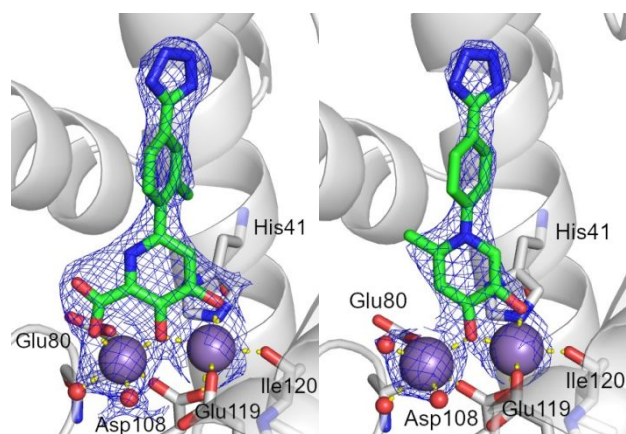


6
7
8
9
10
11
12
13
14
15
16
17
18
19
20
21
22
23
24
25

X-ray Crystallography. A subset of inhibitors was co-crystallized with PA_N endonuclease to elucidate the binding mode for these particularly potent compounds. Tables of data collection and refinement statistics for X-ray structures of PA_N endonuclease bound with compounds **1**, **7**, **13**, **18**, **20**, **22**, **24**, and **40** (Tables S3–S4) as well as figures displaying the electron density of each inhibitor within the protein (Figure S3) are provided in the Supporting Information. In the ligand-free structure, the Mn²⁺ ions are coordinated by amino acid sidechains and water molecules to achieve an octahedral coordination geometry for each metal ion. Inhibitor molecules based on compound **1** were found to coordinate to both Mn²⁺ metal centers by displacing the three coordinated water molecules found in the ligand-free structure with a triad of chelating oxygen atoms, including a carbonyl (coordinating to Mn₁), a hydroxyl (bridging Mn₁ and Mn₂), and a carboxylate (coordinating to Mn₂), as exemplified with compounds **1** (Figure 1) and **22** (Figure 3). This binding motif was elaborated from the bidentate chelation of compound **40** (previously reported as compound Credille-63, Figure 3), the activity of which was previously reported (Table 4),²⁷ but no structure was available. The protein-bound structure of **40** was solved (Figure 3), which shows bidentate coordination of the ligand to Mn₁, but only a monodentate, bridging ligand to Mn₂ (Figure 1).

26
27
28
29
30
31
32
33
34

The inhibitors developed in this study, which bind both Mn²⁺ metal centers, are observed to make two specific types of contacts with PA_N endonuclease: van der Waals interactions with the side wall of the active site near Ile38 via 2'-alkyl substituents (i.e., **7**, **13**, **22**, **24**) and/or contacts with basic active site residues (i.e., **18**, **20**, **24**). With respect to the latter, acidic 3'- and 4'-substituents were observed to make favorable hydrogen bonding interactions (or solvent-mediated hydrogen bonding interactions) with Lys34, Arg124, and/or Arg196 (compounds **18**, **20**, **24**; Figure 4 and Figure S3).



49
50
51
52
53
54
55

Figure 3. Compounds **22** (left, PDB 6E6W) and **40** (right, PDB 6E6X) bound to the PA_N endonuclease active site. In both panels, the protein backbone is shown in gray cartoon. Mn²⁺ ions and water molecules are shown as purple and red spheres, respectively. Residues coordinating the Mn²⁺ ions are shown in sticks, and metal coordination bonds are shown in dashed yellow lines. The electron density of each inhibitor (green sticks) and the Mn²⁺ ions is displayed as a blue mesh contoured to 1.5 σ .

The van der Waals contact with Ile38 has not been previously identified. The benefit of this contact is demonstrated by comparing co-crystal structures of compounds **7** (2'-methyl) and **13** (2'-ethyl) as shown in Figure 4. Extending the methyl group to an ethyl group causes compound **13** to tilt slightly outward so that the terminal carbon of the 2'-ethyl group makes the same van der Waals contacts as the 2'-methyl group in compound **7**. This contact is maintained despite sacrificing favorable, highly enthalpic metal binding interactions; deviations from ideal coordination angle and geometry have previously been shown to have pronounced negative effects on the binding affinity of metal binding inhibitors.³⁷ Larger 2'-substituents (e.g., **9**, **12**) would require an even greater outward tilt to maintain the same van der Waals contact, and this likely contributes to the lower affinity of compounds with larger 2'-substituents (Table 1).

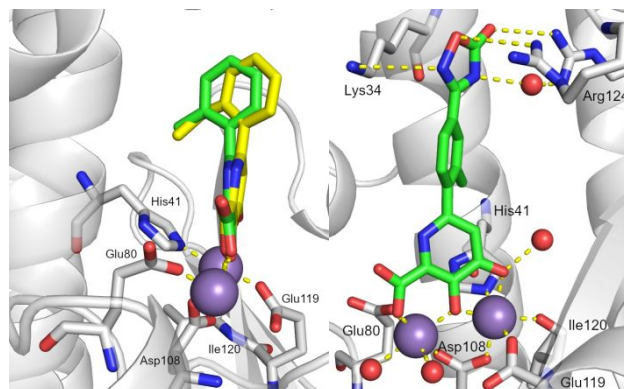


Figure 4. Left: Compounds **7** (green, PDB 6E3N) and **13** (yellow, PDB 6E3O) bound in the PA_N endonuclease active site. Compound **13** is tilted slightly outward relative to compound **7** to accommodate the ethyl substituent. Right: Compound **24** (PDB 6E4C) bound in the active site of PA_N endonuclease makes several solvent-mediated or direct hydrogen bonding interactions with Lys34, Arg124, and/or Arg196. Mn²⁺ ions and water molecules are shown in purple and red spheres, respectively. Metal-coordination and hydrogen bonds are represented with dashed yellow lines.

The protein-bound X-ray structure of compound **18** shows that 3'-substitution forces the inhibitor to adopt an outward tilt (Figure S4). This is accompanied by a decrease in activity, as demonstrated by comparing the IC₅₀ and ΔT_M values of compounds **17** (4'-acid) and **18** (3'-acid) (Table 2). In compound **18**, the outward tilt of the inhibitor is triggered by favorable hydrogen bonding interactions between the 3'-carboxylic acid moiety and Arg196 and solvent-mediated interactions with Lys34. Compound **17** can make similar interactions without tilting and hence without compromising a more ideal metal binding geometry, which gives a structural basis for its greater inhibitory activity.

Compound **20** occupies the active site in an unexpected way: two inhibitor molecules are present, which form π - π stacking interactions with each other (aryl-aryl distance ~ 3.2 Å). One inhibitor molecule coordinates to the metal ions and tilts outward from the active site pocket similar to compound **18** (Figure S4); the second molecule forms polar contacts with Lys34 and Arg124 through its tetrazole ring. We reason that two molecules occupy the active site because of increased available protein interactions as a π - π stacked system. A similar phenomenon was observed in two previous studies on PA_N endonuclease inhibitors.^{31,38} Such stacked interactions may occur because they mimic the binding conformation of the native nucleic acid substrates of PA_N endonuclease.

Merging favorable 2'- and 4'- structural motifs was found to have an additive effect on inhibitor binding, and the merged inhibitors

22 and **24** were crystallographically observed to maintain the same interactions as parent inhibitors (**7**, **13**, **40**). For example, compound **24** maintains the van der Waals contact near Ile38 and solvent mediated or direct hydrogen bond interactions with Lys34, Arg124, and Arg196 (Figure 4).

Inhibitor Selectivity. To evaluate the selectivity of these inhibitors, compounds **22-24** were cross-screened against several dinuclear and mononuclear human metalloenzyme targets, including carbonic anhydrase II (hCAII), matrix metalloproteinase 12 (MMP-12), arginase I (ArgI), and methionine aminopeptidase (MetAP; Mn²⁺ metalloform) (Table S5). Compounds **22-24** show a high degree of selectivity for PA_N endonuclease over these metalloenzymes. To highlight the selectivity of **22-24** for PA_N endonuclease over other metalloenzymes bearing similar Mn²⁺ metal active sites, two dinuclear Mn²⁺ metalloenzymes (ArgI and MetAP) were cross-screened at 200 μM inhibitor concentration. In these assays, only compound **22** showed appreciable cross-inhibition against MetAP (~44% inhibition) and none of these compounds displayed any significant cross-inhibition against ArgI. Little cross-inhibition was observed against the mononuclear Zn²⁺ metalloenzymes hCAII and MMP-12. Taken together, this data indicates that these PA_N endonuclease inhibitors have a high degree of selectivity for their intended target over other competing metalloenzymes, including those with similar dinuclear Mn²⁺ active sites.

Cytotoxicity and Antiviral Assays. Compounds **14**, **19**, **22**, and **23** were selected for cytotoxicity and antiviral activity assays. These assays were carried out in MDCK cells using influenza A H1N1 virus obtained from the American Tissue Culture Collection (A/California/04/2009 H1N1, ATCC VR-1737, see ESI for details). Briefly, 80% confluent MDCK cells were incubated for a period of 48 h at 37 °C 5% CO₂ in the presence of varying concentrations of inhibitor and influenza A virus at a theoretical multiplicity of infection (MOI) of 0.05. After incubation, cells were analyzed for CPE and viability using a CellTiter-Glo (Promega) luminescence assay. Compounds **14** and **19** both showed modest antiviral activity (EC₅₀ = 10.4 ± 2.1 μM and 7.7 ± 3.3 μM, respectively), the positive control L-742,001 exhibited anti-viral activity that is close to our compound (EC₅₀ = 7.4 ± 2.3 μM). The more active compounds **22** and **23** showed similar antiviral activity (EC₅₀ = 21.3 ± 4.8 μM and 11.5 ± 1.2 μM, respectively). While these antiviral activity values are respectable, the large disparity between the in vitro PA_N endonuclease inhibitory activity and cell based antiviral activity indicate that these compounds are likely limited by cellular uptake and permeance, solubility, or other physicochemical attributes. The other positive control Baloxavir acid showed antiviral activity (EC₅₀ = 2.2 ± 0.78 nM) that is significantly higher than L-742,001 and our compounds. However, Baloxavir acid also demonstrated much higher cytotoxicity than the other compounds studied here (~20 μM vs. >800 μM).

Cytotoxicity assays with MDCK cells (the host cell line for the H1N1 virus) and 3T3 cells (a healthy cell line) were also performed. All the tested compounds show nearly no influence on cell viability at doses as high as 800 μM, indicating very low cytotoxicity (Table S6). The selectivity index was determined as the ratio of the concentration of the compound that reduced cell viability to 50% (CC₅₀) to the concentration of the compound needed to inhibit the cytopathic effect to 50% of the control value (EC₅₀). All the compounds showed good selectivity indices (~35-75), with the most potent inhibitor against H1N1 infected MDCK cells, compound **19**, giving a selectivity index of >100. The results reveal excellent selectivity of these inhibitors towards virus over the host cells. Efforts to improve cellular antiviral activity through pro-drugging and isostere strategies are currently underway.

CONCLUSIONS

Based on an optimized MBP inhibitor core, a structure-guided FBDD campaign was employed to generate highly active inhibitors of PA_N endonuclease. Structural elaborations of the optimized MBP core identified key SAR trends, resulting in the development of compounds with activity below the detection limit (IC₅₀ < 2 nM) of the commonly used fluorescence quenching-based endonuclease assay. DSF experiments were employed to further analyze inhibitor binding, and a correlation between nuclease assay inhibition values with Δ*T*_M data was observed. X-ray co-crystal structures of tight binding inhibitors highlight important protein interactions necessary for tight binding. Key structural moieties were merged to create inhibitors with subnanomolar inhibitory activity against PA_N endonuclease, while maintaining a high degree of selectivity for PA_N over similar metalloenzymes.

The lead compounds reported here are among the most active inhibitors of PA_N endonuclease reported in vitro. Even considering that our in vitro nuclease assay tends to yield more potent IC₅₀ values of reported inhibitors (vide supra), compounds **21-24** are still among the most active PA_N endonuclease inhibitors reported to date.^{26,27,31,39} Importantly, compounds **21-24** are far more active and ligand efficient than our previously reported inhibitors,²⁷ showing that our FBDD approach, when combined with biophysical and structural methods, can lead to substantial improvements in in vitro potency.

Overall, the activity and LE of compounds **21-24** are very good. However, relative to their very high in vitro activity, this class of compounds has only modest performance against live virus in cell-saving assays. This may be due to poor cell permeance and cell uptake of these compounds (originating from the presence of three ionizable functional groups), poor solubility, or other physicochemical limitations. Nevertheless, the in vitro activity and LE of these inhibitors indicates that they are good candidates for pro-drugging and isostere strategies to improve cell permeance with more lipophilic structural elaborations.

EXPERIMENTAL

General Experimental Details

All solvents and reagents, unless otherwise noted, were obtained from commercial sources and used without further purification. All reactions, unless otherwise stated, were performed under a nitrogen atmosphere. Silica chromatography was performed using a CombiFlash Rf Teledyne ISCO system using hexane, ethyl acetate, methylene chloride, or methanol as eluents. C18 reverse phase chromatography was performed using the same instrument using 0.1% formic acid in methanol, acetonitrile, or water as eluent. Separations were monitored by mass spectrometry via a Teledyne ISCO RF⁺ PuriIon ESI-MS detector with 1 Da resolution. ¹H and ¹³C NMR spectra were obtained on a Varian (400 MHz) spectrometer or Jeol (500 MHz) spectrometer or a VX (500 MHz) equipped with XSENS cold probe (Varian) spectrometer in the Department of Chemistry and Biochemistry at U.C. San Diego. The purity of all compounds used in assays was determined to be ≥95% by HPLC analysis. Standard resolution MS was performed either at U.C. San Diego Molecular Mass Spectrometry Facility or on the aforementioned Teledyne ISCO RF⁺ PuriIon MS. HRMS analysis was performed using an Agilent 6230 Accurate-Mass LC-TOFMS located at the U.C. San Diego Molecular Mass Spectrometry Facility.

3-Hydroxy-6-methyl-4-oxo-1,4-dihydropyridine-2-carboxylic acid (1). Synthesis of compound **1** was reported previously.²² ¹H NMR (400 MHz, DMSO-*d*₆): δ 6.92 (s, 1H), 2.48 – 2.38 (m, 3H). ¹³C NMR (126 MHz, DMSO-*d*₆): δ 174.66 (s), 166.15 (s), 164.07 (s), 149.36 (s), 135.69 (s), 112.39 (s), 20.07 (d, *J* = 4.3 Hz). HR-

ESI-MS Experimental: 168.0302. Calculated for $[C_7H_6NO_4]^-$: 168.0302. $\Delta = 0.0$ ppm.

4,6-Dibromo-3-hydroxypicolonitrile (2). In a rapidly stirring biphasic solution of EtOAc (50 mL) and H₂O (12.5 mL) was suspended ammonium acetate (14.0 g, 181 mmol) and KCN (4.2 g, 63 mmol). Furfural (5 mL, 60 mmol) was added slowly at room temperature, and the mixture stirred over-night. *A solution of sodium thiosulfate should always be on hand when using KCN as a means to quench cyanide in case of spill or splash, or to decontaminate glassware, funnels, etc. after use.* The reaction mixture was then diluted with 25 mL of saturated sodium bicarbonate solution, and the two layers were separated. After phase separation, the organic layer was extracted once with 50 mL of 5% aqueous HBr with agitation and frequent venting. The organic layer was then further extracted with 2×20 mL of H₂O. The combined aqueous layers were combined and cooled to ~5 °C and Br₂ (12.4 mL, 241 mmol) was added dropwise maintaining the reaction in an ice bath. After addition, the mixture was allowed to warm to room temperature and was stirred overnight and a yellow precipitate formed. The reaction mixture was then cooled to 5-10 °C and 25 mL of a 25% aqueous solution of NaHSO₃ was added slowly, maintaining the reaction mixture on an ice bath, to quench excess Br₂. The resulting suspension was stirred for 30 min then filtered. The filter cake was washed twice with H₂O and dried. The desired product **2** was isolated as a tan solid (8.4 g, 30 mmol, 50% yield; small quantities of a mono-brominated species may be detected by NMR). ¹H NMR (400 MHz, DMSO-*d*₆): δ 8.25 (q, *J* = 0.7 Hz, 1H). HR-ESI-MS Experimental: 274.8459. Calculated for $[C_6HBr_2N_2O]^-$: 274.8461. $\Delta = -0.7$ ppm.

4-(Benzyloxy)-6-bromo-3-hydroxypicolonitrile (3). In a flame-dried flask NaH (2.5 g, 63 mmol) was stirred in dry DMSO (20 mL, dried on molecular sieves). Benzyl alcohol (9.4 mL, 90 mmol) was added dropwise to the mixture, pausing when excessive foam formed. When the reaction was complete, as evidenced by the cessation of hydrogen evolution, compound **2** (5 g, 18 mmol) in dry DMSO (10 mL) was added dropwise to the stirring solution and the mixture was heated to 60 °C for 18 h, monitoring conversion by TLC. When the reaction was complete, the mixture was placed in an ice bath and 150 mL water was added. The mixture continued to stir for 10 min, during which time the solution clouded and then clarified. To remove residual benzyl alcohol, the aqueous solution was extracted with 2×25 mL portions of diethyl ether. Residual ether was then removed from the aqueous portion under vacuum and the solution was cooled to 5 °C on ice. The addition of 4M HCl (until pH ~2) resulted in the precipitation of a white solid. Note, it is imperative to maintain ice bath temperature during acidification; otherwise, excess heat or residual ether present in the solution will result in the formation of a gummy, orange oil in lieu of off-white crystallites. If an oil forms, it can be slowly dissolved in basic (pH >10) water with sonication to repeat the precipitation. The acidified mixture was stirred for 30 min on ice and the resultant solids were filtered, rinsed with H₂O, and dried. Purification via silica gel chromatography in an EtOAc/hexanes system afforded the desired product **3** as an off-white solid (4.2 g, 13.7 mmol, 76% yield). ¹H NMR (400 MHz, acetone-*d*₆): δ 10.38 (s, 1H), 7.51 (d, *J* = 6.5 Hz, 2H), 7.47 – 7.35 (m, 4H), 5.30 (s, 2H). HR-ESI-MS Experimental: 302.9771. Calculated for $[C_{13}H_8BrN_2O_2]^-$: 302.9775. $\Delta = -1.3$ ppm.

General procedure for the synthesis of 4a-24a

Compound **3** (250 mg, 0.8 mmol), SPhos (35 mg, 0.08 mmol), K₂CO₃ (340 mg, 2.4 mmol), and desired boronic acid (1.6 mmol) were dissolved in a 3:1 solution of dioxane:H₂O (20 mL). This solution was de gassed under reduced pressure with stirring for 15

min. [1,1'-Bis(diphenylphosphino)ferrocene]palladium(II) dichloride (30 mg, 5 mol%) was then added and the mixture was heated to 95-100 °C for 18-48 h under nitrogen. The reaction progress was monitored by TLC. Upon completion, the reaction mixture was filtered through a pad of celite and was rinsed once with a 3:1 solution of dioxane:H₂O. The filtrate was acidified to pH<2 with 4M HCl and was concentrated under reduced pressure. The isolated solids were then purified by silica chromatography. However, in a majority of instances, the desired product compound (identified by in-line MS detection and ¹H NMR) was co-purified with residual boronic acid as a significant contaminant, and occasionally co-purified with significant quantities of other starting materials. No further purification was attempted for these compounds as experiments indicated that immediate deprotection of contaminated materials provided a more reliable route for purification and did not significantly impede the subsequent deprotection reaction or purification. Intermediate yields, as determined by ¹H NMR spectroscopy varied from 30-77%.

General procedure for the synthesis of 4-24

Purified or unpurified benzyl protected precursor compound (**4a-24a**) were taken up in a 5:5:1 mixture of concentrated HCl:HOAc:TFA (22 mL total volume) and was heated with stirring to 95 °C for 36-48 h. Reaction progress was monitored by TLC and staining with a solution of FeCl₃ (with the resulting deprotected pyridinone compounds staining with FeCl₃ as a pink-to-red spot on TLC plates). After full deprotection solvents were removed under high vacuum and the resulting solids were co-evaporated several times with MeOH. The remaining solids were then purified by C18 chromatography eluting in a H₂O/MeOH system to yield the target compounds as off-white to lightly pink solids.

3-Hydroxy-4-oxo-6-phenyl-1,4-dihydropyridine-2-carboxylic acid (4).

Compound **4** was prepared according to the general procedure and was isolated as a pink solid in 68% yield. ¹H NMR (400 MHz, DMSO-*d*₆): δ 7.81-7.73 (m, 2H), 7.48 (dd, *J* = 4.1, 2.3 Hz, 3H), 7.31 (s, 1H). ¹³C NMR (126 MHz, DMSO-*d*₆): δ 166.8, 151.5, 145.2, 134.0, 130.4, 129.0, 128.4, 127.6, 112.0. HR-ESI-MS Experimental: 230.0458. Calculated for $[C_{12}H_8NO_4]^-$: 230.0459. $\Delta = -1.4$ ppm.

3-Hydroxy-4-oxo-6-(p-tolyl)-1,4-dihydropyridine-2-carboxylic acid (5).

Compound **5** was prepared according to the general procedure and was isolated as a white solid in 62% yield. ¹H NMR (400 MHz, DMSO-*d*₆): δ 7.67 (d, *J* = 8.1 Hz, 2H), 7.34 – 7.26 (m, 3H), 2.36 (s, 3H). ¹³C NMR (126 MHz, DMSO-*d*₆): δ 166.5, 161.4, 151.6, 144.9, 140.3, 130.9, 129.6, 128.3, 127.3, 111.7, 21.4. HR-ESI-MS Experimental: 244.0615. Calculated for $[C_{13}H_{10}NO_4]^-$: 244.0615. $\Delta = 0.0$ ppm.

3-Hydroxy-4-oxo-6-(m-tolyl)-1,4-dihydropyridine-2-carboxylic acid (6).

Compound **6** was prepared according to the general procedure and was isolated as a light-pink solid in 68% yield. ¹H NMR (400 MHz, DMSO-*d*₆): δ 7.60 (s, 1H), 7.54 (d, *J* = 7.5 Hz, 1H), 7.37 (t, *J* = 7.6 Hz, 1H), 7.30 (d, *J* = 4.4 Hz, 2H), 2.37 (s, 3H). ¹³C NMR (126 MHz, DMSO-*d*₆): δ 166.5, 161.2, 151.7, 145.0, 138.3, 133.65, 131.1, 129.0, 127.4, 125.5, 111.9, 21.4. HR-ESI-MS Experimental: 244.0615. Calculated for $[C_{13}H_{10}NO_4]^-$: 244.0615. $\Delta = 0.0$ ppm.

3-Hydroxy-4-oxo-6-(o-tolyl)-1,4-dihydropyridine-2-carboxylic acid (7).

Compound **7** was prepared according to the general procedure and was isolated as a white solid in 57% yield. ¹H NMR (400 MHz, DMSO-*d*₆): δ 7.39 (t, *J* = 7.9 Hz, 1H), 7.35 – 7.24 (m, 3H), 6.98 (s, 1H), 2.18 (s, 3H). ¹³C NMR (126 MHz, DMSO-*d*₆): δ 165.1, 162.4, 152.2, 144.5, 136.7, 130.6, 130.2, 130.1, 126.8,

126.1, 113.94, 20.0. HR-ESI-MS Experimental: 244.0614. Calculated for $[C_{13}H_{10}NO_4]^-$: 244.0615. $\Delta = -0.4$ ppm.

3-Hydroxy-6-(3-isopropylphenyl)-4-oxo-1,4-dihydropyridine-2-carboxylic acid (8). Compound **8** was prepared according to the general procedure and was isolated as a white solid in 51% yield. 1H NMR (400 MHz, DMSO- d_6): δ 7.64 (s, 1H), 7.58 – 7.51 (m, 1H), 7.45 – 7.34 (m, 2H), 7.31 (s, 1H), 2.97 (s, 1H), 1.24 (dd, $J = 6.9, 1.6$ Hz, 6H). ^{13}C NMR (126 MHz, DMSO- d_6): δ 166.4, 161.4, 151.7, 149.2, 145.2, 133.6, 129.1, 128.5, 127.4, 126.6, 125.9, 112.04, 33.9, 24.2. HR-ESI-MS Experimental: 272.0927. Calculated for $[C_{15}H_{14}NO_4]^-$: 272.0928. $\Delta = -0.4$ ppm.

3-Hydroxy-6-(2-isopropylphenyl)-4-oxo-1,4-dihydropyridine-2-carboxylic acid (9). Compound **9** was prepared according to the general procedure and was isolated as a white solid in 56% yield. 1H NMR (400 MHz, CDCl₃): δ 7.36 (m, 1H), 7.18 (dd, $J = 6.4, 1.5$ Hz, 2H), 6.98 (s, 1H), 2.97 (dq, $J = 13.3, 6.7$ Hz, 1H), 1.19 – 1.04 (m, 6H). ^{13}C NMR (126 MHz, DMSO- d_6): δ 165.2, 162.4, 152.2, 147.1, 144.6, 132.8, 130.5, 130.1, 126.7, 125.9, 125.8, 114.1, 30.2, 24.2. HR-ESI-MS Experimental: 272.0926. Calculated for $[C_{15}H_{14}NO_4]^-$: 272.0928. $\Delta = -0.7$ ppm.

3-Hydroxy-4-oxo-6-(4-phenoxyphenyl)-1,4-dihydropyridine-2-carboxylic acid (10). Compound **10** was prepared according to the general procedure and was isolated as a pink solid in 61% yield. 1H NMR (400 MHz, DMSO- d_6): δ 7.79 (d, $J = 8.7$ Hz, 2H), 7.42 (t, $J = 7.9$ Hz, 2H), 7.27 (s, 1H), 7.19 (t, $J = 7.4$ Hz, 1H), 7.07 (dd, $J = 8.1, 3.8$ Hz, 4H). ^{13}C NMR (126 MHz, DMSO- d_6): δ 166.9, 160.9, 158.9, 156.3, 151.3, 144.7, 130.7, 130.3, 129.0, 127.5, 124.6, 119.8, 118.4, 111.6. HR-ESI-MS Experimental: 322.0715. Calculated for $[C_{18}H_{12}NO_5]^-$: 322.0721. $\Delta = -1.9$ ppm.

3-Hydroxy-4-oxo-6-(3-phenoxyphenyl)-1,4-dihydropyridine-2-carboxylic acid (11). Compound **11** was prepared according to the general procedure and was isolated as a white solid in 67% yield. 1H NMR (400 MHz, DMSO- d_6): δ 7.84 (s, 1H), 7.61 – 7.35 (m, 5H), 7.18 – 6.93 (m, 4H). ^{13}C NMR (126 MHz, DMSO- d_6): δ 167.9, 157.0, 157.0, 151.2, 144.6, 137.2, 130.8, 130.6, 124.1, 123.9, 123.0, 120.1, 119.1, 119.0, 118.4, 111.9. HR-ESI-MS Experimental: 322.0720. Calculated for $[C_{18}H_{12}NO_5]^-$: 322.0721. $\Delta = -0.3$ ppm.

3-Hydroxy-4-oxo-6-(2-phenoxyphenyl)-1,4-dihydropyridine-2-carboxylic acid (12). Compound **12** was prepared according to the general procedure and was isolated as a white solid in 54% yield. 1H NMR (400 MHz, DMSO- d_6): δ 7.64 (d, $J = 7.7$ Hz, 1H), 7.50 (t, $J = 7.8$ Hz, 1H), 7.34 (t, $J = 7.8$ Hz, 2H), 7.27 (t, $J = 7.5$ Hz, 1H), 7.21 (s, 1H), 7.10 (t, $J = 7.4$ Hz, 1H), 7.01 – 6.95 (m, 3H). ^{13}C NMR (126 MHz, DMSO- d_6): δ 165.3, 161.9, 156.4, 154.4, 152.0, 140.8, 132.4, 131.8, 130.5, 126.8, 124.8, 124.3, 124.2, 119.3, 119.0, 113.8. HR-ESI-MS Experimental: 322.0717. Calculated for $[C_{18}H_{12}NO_5]^-$: 322.0721. $\Delta = -1.2$ ppm.

6-(2-Ethylphenyl)-3-hydroxy-4-oxo-1,4-dihydropyridine-2-carboxylic acid (13). Compound **13** was prepared according to the general procedure and was isolated as a light pink solid in 52% yield. 1H NMR (400 MHz, DMSO- d_6): δ 7.46 – 7.39 (m, 1H), 7.34 (d, $J = 7.5$ Hz, 1H), 7.30 – 7.26 (m, 2H), 6.98 (s, 1H), 2.52 – 2.46 (m, 2H), 1.01 (t, $J = 7.6$ Hz, 3H). ^{13}C NMR (126 MHz, DMSO- d_6): δ 165.2, 162.2, 152.2, 144.6, 142.6, 133.2, 130.4, 130.2, 128.8, 126.8, 126.0, 114.0, 26.0, 15.5. HR-ESI-MS Experimental: 258.0771. Calculated for $[C_{14}H_{12}NO_4]^-$: 258.0772. $\Delta = -0.4$ ppm.

3-Hydroxy-4-oxo-6-(2-(trifluoromethyl)phenyl)-1,4-dihydropyridine-2-carboxylic acid (14). Compound **14** was

prepared according to the general procedure and was isolated as a dark pink solid in 55% yield. 1H NMR (500 MHz, DMSO- d_6): δ 7.83 (d, $J = 7.5$ Hz, 1H), 7.72 (dd, $J = 12.2, 7.5$ Hz, 2H), 7.58 (d, $J = 7.2$ Hz, 1H), 7.01 (s, 1H). ^{13}C NMR (126 MHz, DMSO- d_6): δ 165.8, 161.6, 152.4, 142.4, 132.9, 132.6, 132.4, 130.6, 127.8 (q, $J = 30.1$ Hz, 1C), 127.1, 126.4 (q, $J = 4.8$ Hz, 1C), 124.2 (q, $J = 27.7$ Hz, 1C), 114.1. HR-ESI-MS Experimental: 298.0329. Calculated for $[C_{13}H_7F_3NO_4]^-$: 298.0333. $\Delta = -1.3$ ppm.

3-Hydroxy-6-(2-methoxyphenyl)-4-oxo-1,4-dihydropyridine-2-carboxylic acid (15). Compound **15** was prepared according to the general procedure and was isolated as a white solid in 39% yield. 1H NMR (400 MHz, DMSO- d_6): δ 7.58 (d, $J = 7.7$ Hz, 1H), 7.51 (t, $J = 8.4$ Hz, 1H), 7.27 (s, 1H), 7.21 (d, $J = 8.4$ Hz, 1H), 7.09 (t, $J = 7.6$ Hz, 1H), 3.87 (s, 3H). ^{13}C NMR (126 MHz, DMSO- d_6): δ 164.9, 162.7, 157.3, 151.9, 141.0, 132.7, 130.6, 125.9, 121.4, 120.43, 112.8, 112.6, 56.6. HR-ESI-MS Experimental: 260.0563. Calculated for $[C_{13}H_{10}NO_5]^-$: 260.0564. $\Delta = -0.4$ ppm.

3-Hydroxy-6-(2-(methylthio)phenyl)-4-oxo-1,4-dihydropyridine-2-carboxylic acid (16). Compound **16** was prepared according to the general procedure and was isolated as a white solid in 56% yield. 1H NMR (400 MHz, DMSO- d_6): δ 7.48 (dd, $J = 11.3, 3.7$ Hz, 1H), 7.41 (d, $J = 7.9$ Hz, 1H), 7.36 – 7.32 (m, 1H), 7.26 (t, $J = 7.4$ Hz, 1H), 7.02 (s, 1H), 2.41 (s, 3H). ^{13}C NMR (126 MHz, DMSO- d_6): δ 165.3, 161.8, 152.5, 143.3, 138.2, 132.9, 130.9, 130.6, 127.0, 126.6, 125.2, 114.2, 16.0. HR-ESI-MS Experimental: 276.0333. Calculated for $[C_{13}H_{10}NO_4S]^-$: 276.0336. $\Delta = -1.1$ ppm.

6-(4-Carboxyphenyl)-3-hydroxy-4-oxo-1,4-dihydropyridine-2-carboxylic acid (17). Compound **17** was prepared according to the general procedure and was isolated as a pink solid in 22% yield. 1H NMR (400 MHz, DMSO- d_6): δ 7.98 (q, $J = 8.4$ Hz, 4H), 7.32 (s, 1H). ^{13}C NMR (126 MHz, DMSO- d_6): δ 168.7, 167.4, 159.0, 151.0, 144.7, 139.9, 131.5, 129.9, 129.3, 127.8, 112.0. HR-ESI-MS Experimental: 274.0356. Calculated for $[C_{13}H_8NO_6]^-$: 274.0357. $\Delta = -0.4$ ppm.

6-(3-Carboxyphenyl)-3-hydroxy-4-oxo-1,4-dihydropyridine-2-carboxylic acid (18). Compound **18** was prepared according to the general procedure and was isolated as a pink solid in 43% yield. 1H NMR (400 MHz, DMSO- d_6): δ 8.33 (s, 1H), 8.03 (dd, $J = 16.0, 7.8$ Hz, 2H), 7.60 (t, $J = 7.8$ Hz, 1H), 7.37 (s, 1H). ^{13}C NMR (126 MHz, DMSO- d_6): δ 167.8, 167.4, 159.7, 151.1, 144.8, 135.4, 132.3, 131.4, 130.6, 129.4, 129.0, 128.6, 112.0. HR-ESI-MS Experimental: 274.0359. Calculated for $[C_{13}H_8NO_6]^-$: 274.0357. $\Delta = 0.8$ ppm.

6-(4-(1H-tetrazol-5-yl)phenyl)-3-hydroxy-4-oxo-1,4-dihydropyridine-2-carboxylic acid (19). Compound **19** was prepared according to the general procedure and was isolated as a white solid in 31% yield. 1H NMR (400 MHz, DMSO- d_6): δ 8.11 (q, $J = 8.2$ Hz, 4H), 7.45 (s, 1H). ^{13}C NMR (126 MHz, DMSO- d_6): δ 168.6, 158.9, 151.0, 144.7, 138.2, 129.0, 128.6, 127.5, 125.2, 112.0, 40.9. HR-ESI-MS Experimental: 320.0398. Calculated for $[C_{13}H_7N_5O_4Na]^-$: 320.0401. $\Delta = -0.9$ ppm.

6-(3-(1H-tetrazol-5-yl)phenyl)-3-hydroxy-4-oxo-1,4-dihydropyridine-2-carboxylic acid (20). Compound **20** was prepared according to the general procedure and was isolated as a light pink solid in 38% yield. 1H NMR (500 MHz, DMSO- d_6): δ 8.51 (d, $J = 25.9$ Hz, 1H), 8.23 – 7.99 (m, 2H), 7.78 (d, $J = 28.4$ Hz, 1H), 7.46 (s, 1H). HR-ESI-MS Experimental: 320.0397. Calculated for $[C_{13}H_7N_5O_4Na]^-$: 320.0401. $\Delta = -1.3$ ppm.

6-(4-Carboxy-2-methylphenyl)-3-hydroxy-4-oxo-1,4-dihydropyridine-2-carboxylic acid (21). Compound **21** was prepared according to the general procedure and was isolated as a white solid in 21% yield. ¹H NMR (400 MHz, DMSO-*d*₆): δ 7.85 (s, 1H), 7.81 (d, *J* = 8.4 Hz, 1H), 7.44 (d, *J* = 7.7 Hz, 1H), 6.98 (s, 1H), 2.24 (s, 3H). ¹³C NMR (126 MHz, DMSO-*d*₆): δ 167.4, 165.5, 162.2, 152.3, 149.0, 143.7, 138.1, 137.3, 132.0, 131.2, 130.5, 126.8, 113.8, 19.9. HR-ESI-MS Experimental: 288.0512. Calculated for [C₁₄H₁₀NO₆]⁻: 288.0514. Δ = -0.7 ppm.

3-Hydroxy-6-(2-methyl-4-(1H-tetrazol-5-yl)phenyl)-4-oxo-1,4-dihydropyridine-2-carboxylic acid (22). Compound **22** was prepared according to the general procedure and was isolated as a white solid in 24% yield. ¹H NMR (400 MHz, DMSO-*d*₆): δ 7.98 (s, 1H), 7.92 (d, *J* = 8.0 Hz, 1H), 7.55 (d, *J* = 7.9 Hz, 1H), 6.97 (s, 1H), 2.30 (s, 3H). ¹³C NMR (126 MHz, DMSO-*d*₆): δ 165.7, 163.0, 155.6, 152.3, 143.6, 138.2, 136.6, 131.3, 128.9, 126.9, 125.7, 124.6, 114.0, 20.1. HR-ESI-MS Experimental: 312.0735. Calculated for [C₁₄H₁₀N₅O₄]⁻: 312.0738. Δ = -1.0 ppm.

3-Hydroxy-6-(2-(trifluoromethyl)-4-(1H-tetrazol-5-yl)phenyl)-4-oxo-1,4-dihydropyridine-2-carboxylic acid (23). Compound **23** was prepared according to the general procedure and was isolated as a white solid in 29% yield. ¹H NMR (400 MHz, DMSO-*d*₆): δ 8.45 (s, 1H), 8.39 (d, *J* = 8.0 Hz, 1H), 7.85 (d, *J* = 8.0 Hz, 1H), 7.10 (s, 1H). ¹³C NMR (126 MHz, DMSO-*d*₆): δ 166.8, 162.7, 156.5, 152.2, 141.9, 135.4, 133.5, 130.2, 128.6 (q, *J* = 30.4 Hz, 1C), 124.2 (q, *J* = 5.0 Hz, 1C), 123.9 (q, *J* = 274.3 Hz, 1C), 114.1, 66.8. HR-ESI-MS Experimental: 366.0450. Calculated for [C₁₄H₇F₃N₅O₄]⁻: 366.0456. Δ = -1.6 ppm.

3-Hydroxy-6-(2-methyl-4-(5-oxo-4,5-dihydro-1,2,4-oxadiazol-3-yl)phenyl)-4-oxo-1,4-dihydropyridine-2-carboxylic acid (24). Compound **24** was prepared according to the general procedure and was isolated as a white solid in 36% yield. ¹H NMR (400 MHz, DMSO-*d*₆): δ 8.31 (s, 1H), 8.19 (s, 1H), 7.74 (s, 1H), 7.69 (d, *J* = 7.8 Hz, 1H), 7.59 (d, *J* = 8.1 Hz, 1H), 7.09 (s, 1H), 2.40 (s, 3H). ¹³C NMR (126 MHz, DMSO-*d*₆): δ 172.5, 160.4, 160.4, 157.6, 154.2, 148.8, 147.7, 143.3, 137.4, 130.7, 130.6, 128.5, 124.0, 123.0, 115.0, 20.8. HR-ESI-MS Experimental: 328.0571. Calculated for [C₁₅H₁₀N₃O₆]⁻: 328.0575. Δ = -1.2 ppm.

3-Methyl-4-(4,4,5,5-tetramethyl-1,3,2-dioxaborolan-2-yl)benzoic acid (25). In a 30 mL microwave vessel were combined 4-bromo-3-methylbenzoic acid (1.0 g, 4.6 mmol), bis(pinacolato)diboron (1.77 g, 6.9 mmol), potassium acetate (1.14 g, 11.6 mmol), and Pd(dppf)Cl₂ (0.38 g, 0.46 mmol) in dry DMF (10 mL). The reaction mixture was heated to 125 °C for 20 min in a microwave reactor. After heating, the solvent was removed under vacuum and the residue was taken up in 2M HCl and EtOAc. The layers were separated and the aqueous phase was extracted once with EtOAc. Combined organic fractions were dried and concentrated to yield a brown oil, which was purified by silica chromatography (EtOAc:hexanes) to produce **25** as a white solid in 74% yield (900 mg, 3.4 mmol). Evidence of hydrolysis products of the boronic ester were observed in the NMR spectrum but were found to still be useful in the subsequent coupling reaction. ¹H NMR (500 MHz, CD₃OD): δ 7.80 (s, 1H), 7.77 (d, *J* = 0.96 Hz, 2H), 2.55 (s, 3H), 1.36 (s, 12H). HR-ESI-MS Experimental: 261.1308. Calculated for [C₁₄H₁₈BO₄]⁻: 261.1306. Δ = 0.8 ppm.

3-Methyl-4-(4,4,5,5-tetramethyl-1,3,2-dioxaborolan-2-yl)benzonitrile (26). In a microwave vessel were combined 4-bromo-3-methylbenzonitrile (1.0 g, 5.1 mmol), bis(pinacolato)diboron (1.94 g, 7.6 mmol), potassium acetate (1.25 g, 12.7 mmol), and Pd(dppf)Cl₂ (0.41 g, 0.51 mmol) in dry DMF

(10 mL). The reaction mixture was heated to 125 °C for 20 min in a microwave reactor. After heating, the solvent was removed under vacuum and the residue was taken up in 2M HCl and EtOAc. The layers were separated and the aqueous phase was extracted once with EtOAc. The combined organic fractions were dried and concentrated to yield a brown oil, which was purified by silica chromatography (EtOAc:hexanes) to produce **26** as a white solid in 89% yield (1.1 g, 4.5 mmol). ¹H NMR (500 MHz, CD₃OD): δ 7.83 (d, *J* = 7.7 Hz, 1H), 7.52 (s, 1H), 7.49 (d, *J* = 7.7 Hz, 1H), 2.56 (s, 3H), 1.37 (s, 12H). HR-ESI-MS Experimental: 266.1326. Calculated for [C₁₄H₁₈BNO₂Na]⁺: 266.1325. Δ = 0.4 ppm.

5-(3-Methyl-4-(4,4,5,5-tetramethyl-1,3,2-dioxaborolan-2-yl)phenyl)-1H-tetrazole (27). Compound **26** (2.0 g, 8.2 mmol), NH₄Cl (1.32 g, 24.6 mmol), and NaN₃ (0.80 g, 12.3 mmol) were combined in DMF (15 mL) and stirred. The reaction mixture was heated to 110 °C for 3 h. Upon cooling, the mixture was poured into 150 mL of cool water (note: maintain the concentration of azide in solution <5%) and was acidified to pH 2 with 4M HCl. A white precipitate formed and the solution was stirred in an ice bath for 30 min, after which time the solids were collected by filtration and dried to produce **27** as a white solid in 93% yield (2.2 g, 7.6 mmol). ¹H NMR (400 MHz, DMSO-*d*₆): δ 7.85 (s, 1H), 7.80 (t, *J* = 6.6 Hz, 2H), 2.54 (s, 3H), 1.30 (s, 12H). HR-ESI-MS Experimental: 287.1673. Calculated for [C₁₄H₂₀BN₄O₂]⁺: 287.1676. Δ = -1.0 ppm.

4-(4,4,5,5-Tetramethyl-1,3,2-dioxaborolan-2-yl)-3-(trifluoromethyl)benzonitrile (28). In a microwave vessel were combined 4-bromo-3-(trifluoromethyl)benzonitrile (2.6 g, 10.4 mmol), bis(pinacolato)diboron (3.96 g, 15.6 mmol), potassium acetate (2.55 g, 26.0 mmol), and Pd(dppf)Cl₂ (0.85 g, 1.0 mmol) in dry DMF (15 mL). The reaction mixture was heated to 125 °C in a microwave reactor for 25 min. After heating, the solvent was removed under vacuum and the residue was taken up in 2M HCl and EtOAc. The layers were separated and the aqueous phase was extracted once with EtOAc. Combined organic fractions were dried and concentrated to yield a brown oil, which was purified by silica chromatography (EtOAc:hexanes) to produce **28** as a white solid in 66% yield (2.1 g, 6.8 mmol). ¹H NMR (400 MHz, CDCl₃): δ 7.93 (s, 1H), 7.85 (d, *J* = 7.7 Hz, 1H), 7.79 (d, *J* = 7.7 Hz, 1H), 1.37 (s, 12H).

5-(4-(4,4,5,5-Tetramethyl-1,3,2-dioxaborolan-2-yl)-3-(trifluoromethyl)phenyl)-1H-tetrazole (29). Compound **28** (2.0 g, 6.7 mmol), NH₄Cl (1.08 g, 20.2 mmol), and NaN₃ (0.66 g, 10.1 mmol) were combined in DMF (15 mL) and stirred. The reaction mixture was heated to 110 °C for 3 h. Upon cooling, the mixture was poured into 150 mL cool water (note: maintain the concentration of azide in solution <5%) and was acidified to pH 2 with 4M HCl. A white precipitate formed and the solution was stirred in an ice bath for 30 min, after which time the solids were collected by filtration and dried to produce **29** as a white solid in 94% yield (2.15 g, 6.3 mmol). ¹H NMR (400 MHz, DMSO-*d*₆): δ 8.37 (s, 1H), 8.32 (d, *J* = 7.7 Hz, 1H), 7.95 (d, *J* = 7.7 Hz, 1H), 1.32 (d, *J* = 3.0 Hz, 12H). HR-ESI-MS Experimental: 341.1398. Calculated for [C₁₄H₁₇BF₃N₄O₂]⁺: 341.1394. Δ = 1.2 ppm.

4-Bromo-N'-hydroxy-3-methylbenzimidamide (30). To a solution of 4-bromo-3-methylbenzonitrile (2.0 g, 10.2 mmol) in EtOH (20 mL) was added hydroxylamine hydrochloride (1.42 g, 20.4 mmol), and TEA (2.8 mL, 20.4 mmol) with stirring. The reaction mixture was heated to reflux for 3 h, after which time solvent was removed under vacuum and the residue was taken up in 1M HCl. The acidic solution was washed with 40 mL CH₂Cl₂

and cooled in an ice bath with stirring. The pH of the cooled aqueous solution was then adjusted to >10 with 6M NaOH and a white precipitate formed. The basic solution stirred on ice for 30 min and the resultant solids were isolated by filtration to give **30** as a white solid in 77% yield (1.8 g, 7.9 mmol). ¹H NMR (400 MHz, DMSO-*d*₆): δ 9.65 (d, *J* = 6.1 Hz, 1H), 7.61 (s, 1H), 7.55 – 7.50 (m, 1H), 7.38 (dd, *J* = 5.5, 2.8 Hz, 1H), 5.80 (s, 2H), 2.32 (d, *J* = 5.5 Hz, 3H). HR-ESI-MS Experimental: 228.9971. Calculated for [C₈H₁₀BrN₂O]⁺: 228.9971. Δ = 0.0 ppm.

3-(4-Bromo-3-methylphenyl)-1,2,4-oxadiazol-5(4H)-one (31). To a stirring solution of compound **30** (1.0 g, 4.4 mmol) and TEA (0.91 mL, 6.5 mmol) in DMF (10 mL) was added ethyl chloroformate (0.46 mL, 4.8 mmol) dropwise at room temperature. The reaction mixture stirred for 30 min, after which time the mixture was heated to 130 °C for 1.5 h. After heating, the DMF solution was poured into 125 mL of cool water and 25 mL 1M NaOH. The aqueous solution was washed once with CH₂Cl₂ and was cooled in an ice bath with stirring. The basic solution was then acidified with 4M HCl to pH <2. A white solid formed and the solution stirred for 15 min. The solid was then isolated by filtration to produce **31** as a white solid in 63% yield (700 mg, 2.7 mmol). ¹H NMR (400 MHz, DMSO-*d*₆): δ 7.69 (s, 1H), 7.53 (d, *J* = 8.3 Hz, 1H), 7.46 (d, *J* = 8.2 Hz, 1H), 2.32 (s, 3H). HR-ESI-MS Experimental: 252.9618. Calculated for [C₉H₆BrN₂O₂]⁻: 252.9618. Δ = 0.0 ppm.

3-(3-Methyl-4-(4,4,5,5-tetramethyl-1,3,2-dioxaborolan-2-yl)phenyl)-1,2,4-oxadiazol-5(4H)-one (32). In a 30 mL microwave vessel were combined compound **31** (500 mg, 1.96 mmol), bis(pinacolato)diboron (750 mg, 2.95 mmol), potassium acetate (480 mg, 8.1 mmol), and Pd(dppf)Cl₂ (200 mg, 0.25 mmol) in dry DMF (10 mL). The reaction mixture was heated to 125 °C for 20 min in a microwave reactor. The solvent was then evaporated under vacuum and the residue was taken up in 2M HCl and EtOAc. The layers were separated and the aqueous phase was extracted once with EtOAc. The combined organic fractions were dried and concentrated to yield a brown oil, which was purified by silica chromatography (EtOAc:hexanes) to produce **32** as a white solid in 59% yield (350 mg, 1.16 mmol). Evidence of hydrolysis products of the boronic ester were observed in the NMR spectrum but were found to still be useful in the subsequent coupling reaction. ¹H NMR (400 MHz, CD₃OD): δ 7.81 (d, *J* = 7.7 Hz, 1H), 7.59 – 7.47 (m, 2H), 2.54 (s, 3H), 1.35 (s, 12H). HR-ESI-MS Experimental: 301.1366. Calculated for [C₁₅H₁₈BN₂O₄]⁻: 301.1368. Δ = -0.7 ppm.

PA_N Enzymatic Nuclease Activity Assay

PA_N endonuclease activity assays were carried out as previously reported.²⁷ Briefly, assay were performed using Black Costar 96-well plates. Each well contained a total volume of 100 μL comprised of: buffer (20 mM Tris, 150 mM NaCl, 2 mM MnCl₂, 10 mM β-mercaptoethanol, 0.2% Triton-X100, pH 8.0), influenza PA_N endonuclease (5 or 25 nM), inhibitor (various concentrations) in buffer, and fluorescent ssDNA-oligo substrate (200 nM). A single-stranded, 17-mer DNA oligonucleotide labeled with a 5'-FAM fluorophore and a 3'-TAMRA quencher ([6-FAM]AATCGCAGGCAGCACTC[TAM], Sigma-Aldrich) was employed as the substrate. Upon addition of the substrate, the change in fluorescence was measured over 45 min at 37 °C (λ_{ex} = 485 nm; λ_{em} = 528 nm). The gain was set to 100 and the first 15 min of data were excluded from the activity calculations. Dose-response curves were generated, fitted, and analyzed using Origin16 graphing software. For most experiments, the enzyme concentration was 25 nM, which afforded a strong change in

fluorescent signal, but had an IC₅₀ detection limit of ~15 nM. Using an enzyme concentration of 5 nM, the detection limit was observed to be ~2 nM; however, the change in fluorescent signal was significantly weaker than that from an enzyme concentration of 25 nM. These detection limits prompted the use of thermal shift assay to distinguish between the highly potent inhibitors reported herein.

Thermal Shift Assay (DSF)

To each well of a 96-well 0.2 mL optical MicroAmp (ThermoFisher) thermocycler plate was added 9.5 μL of buffer (150 mM NaCl, 2 mM MnCl₂, 20 mM HEPES pH 7.5), 4 μL of PA_N endonuclease in buffer (250 μg/mL), 4 μL of inhibitor in buffer (1 mM; 2% DMSO), and 2.5 μL of 8 × SYPRO orange Thermal Shift[®] dye (ThermoFisher) in buffer. This results in a final well volume of 20 μL containing final concentrations of 1 μg PA_N endonuclease, 200 μM inhibitor, and 1× dye in buffer with 0.4% DMSO. The presence of this small concentration of DMSO was found to have a negligible effect on Δ*T*_M values of native PA_N endonuclease. Thermocycler plate wells were sealed prior to analysis, and the plate was then heated in a thermocycler from 25 °C to 99 °C at a ramp rate of 0.05 °C/sec. Fluorescence was read using the ROX filter channel (λ_x = 580 nm; λ_{em} = 623 nm) and fluorescence signal was fitted to a first derivative curve to identify *T*_M. Native PA_N endonuclease was generally observed to melt with a *T*_M = 58–60 °C. All assayed compounds were observed to cause either no significant Δ*T*_M or a positive Δ*T*_M.

ASSOCIATED CONTENT

Supporting Information

The Supporting Information is available free of charge on the ACS Publications website at DOI:

Synthesis of boronic esters; protein expression and purification; assay data of PA_N endonuclease control inhibitors; protein crystallography; cross-inhibition assays; cell-based assays; NMR spectra of select lead inhibitors.

SMILES strings for all compounds (PDF)

SMILES strings formula (CSV)

PDB file of **1** modeled in PA_N (PDB)

PDB file of **7** modeled in PA_N (PDB)

PDB file of **13** modeled in PA_N (PDB)

PDB file of **18** modeled in PA_N (PDB)

PDB file of **20** modeled in PA_N (PDB)

PDB file of **22** modeled in PA_N (PDB)

PDB file of **24** modeled in PA_N (PDB)

PDB file of **40** modeled in PA_N (PDB)

Corresponding Author

*scohen@ucsd.edu, chenyaoyao@nankai.edu.cn

Notes

S.M.C. is a co-founder, has an equity interest, and receives income as member of the Scientific Advisory Board for Cleave Biosciences and is a co-founder, has an equity interest, and a member of the Scientific Advisory Board for Forge Therapeutics. Both companies may potentially benefit from the research results of certain projects in the laboratory of S.M.C. The terms of this arrangement have been reviewed and approved by the University of California, San Diego in accordance with its conflict of interest policies.

ACCESSION CODES

PDB ID code for protein structures of PA_N endonuclease (compound co-crystallized with protein given in parentheses): 6E6V (compound **1**), 6E3N (compound **7**), 6E3O (compound **13**), 6E3M (compound **18**), 6E3P (compound **20**), 6E6W (compound **22**), 6E4C (compound **24**), 6E6X (compound **40**). Authors will release the atomic coordinates and experimental data upon article publication.

ABBREVIATIONS

ArgI, arginase I; DPBA, 2,4-dioxo-4-phenylbutanoic acid; DSF, differential scanning fluorimetry; EGCG, epigallocatechin gallate; FBDD, fragment-based drug discovery; FDA, U.S. Food and Drug Administration; hCA, human carbonic anhydrase; LE, ligand efficiency; MBP, metal-binding pharmacophore; MetAP, methionine aminopeptidase; MMP, matrix metalloproteinase; PA_N, N-terminal domain of the polymerase acidic (PA) subunit of the RNA-dependent RNA polymerase complex from the influenza A virus; PSA, polar surface area; SAR, structure-activity relationship; SBDD, structure-based drug design;

ACKNOWLEDGMENT

The authors acknowledge Dr. Yongxuan Su (U.C. San Diego, Molecular Mass Spectrometry Facility) for aid with HR-MS and HPLC compound purity analysis; Prof. Carlo Ballatore (U.C. San Diego) for access to a preparative HPLC system; and Dr. Curtis Moore and Dr. Milan Gembicky (UC San Diego X-ray Facility), the Prof. J. P. Noel (Salk Institute), and the staff at beam lines 5.0.1 and 5.0.2 at the Advanced Light Source for assistance with X-ray crystallography studies. This work was supported by grants from the National Institutes of Health (R01 GM098435 to S.M.C.; F32 GM125233 to C.N.M.), and by the University of California President's Postdoctoral Fellowship (to C.N.M.). B.L.D. was supported, in part, by the National Institute of Health Molecular Biophysics Training Grant (T32GM008326-26). R.W.S. was supported, in part, by the Graduate Research Fellowship Program (GRFP) from the National Science Foundation.

REFERENCES

- (1) Nichol, K. L.; Treanor, J. J. Vaccines for Seasonal and Pandemic Influenza. *J. Infect. Dis.* **2006**, *194* (Suppl. 2), S111-118.
- (2) Subbarao, K.; Joseph, T. Scientific Barriers to Developing Vaccines Against Avian Influenza Viruses. *Nat. Rev. Immunol.* **2007**, *7*, 267-278.
- (3) Monod, A.; Swale, C.; Tarus, B.; Tissot, A.; Delmas, B.; Ruigrok, R. W.; Crepin, T.; Slama-Schwok, A. Learning From Structure-Based Drug Design and New Antivirals Targeting the Ribonucleoprotein Complex for the Treatment of Influenza. *Expert Opin. Drug Discov.* **2015**, *10*, 345-371.
- (4) Drake, J. W. Rates of Spontaneous Mutation among RNA Viruses. *Proc. Natl. Acad. Sci. U. S. A.* **1993**, *90*, 4171-4175.
- (5) Watanabe, T.; Kawaoka, Y. Influenza Virus-Host Interactomes as a Basis for Antiviral Drug Development. *Curr. Opin. Virol.* **2015**, *14*, 71-78.
- (6) Li, T. C. M.; Chan, M. C. W.; Lee, N. Clinical Implications of Antiviral Resistance in Influenza. *Viruses* **2015**, *7*, 4929-4944.
- (7) Bright, R. A.; Shay, D. K.; Shu, B.; Cox, N. J.; Klimov, A. I. Adamantane Resistance Among Influenza A Viruses Isolated Early During the 2005-2006 Influenza Season in the United States. *JAMA, J. Am. Med. Assoc.* **2006**, *295*, 891-894.
- (8) Amarelle, L.; Lecuona, E.; Sznajder, J. I. Anti-Influenza Treatment: Drugs Currently Used and Under Development. *Arch. Bronconeumol.* **2017**, *53*, 19-26.
- (9) Collins, P. J.; Haire, L. F.; Lin, Y. P.; Liu, J. F.; Russell, R. J.; Walker, P. A.; Skehel, J. J.; Martin, S. R.; Hay, A. J.; Gamblin, S.

- J. Crystal Structures of Oseltamivir-Resistant Influenza Virus Neuraminidase Mutants. *Nature* **2008**, *453*, 1258-1261.
- (10) Moscona, A. Global Transmission of Oseltamivir-Resistant Influenza. *N. Engl. J. Med.* **2009**, *360*, 953-956.
- (11) Heo, Y. A. Baloxavir: First Global Approval. *Drugs* **2018**, *78*, 693-697.
- (12) Huang, T. S.; Palese, P.; Krystal, M. Determination of Influenza-Virus Proteins Required for Genome Replication. *J. Virol.* **1990**, *64*, 5669-5673.
- (13) Fodor, E. The RNA Polymerase of Influenza A Virus: Mechanisms of Viral Transcription and Replication. *Acta Virol.* **2013**, *57*, 113-122.
- (14) Resa-Infante, P.; Jorba, N.; Coloma, R.; Ortin, J. The Influenza Virus RNA Synthesis Machine: Advances in its Structure and Function. *RNA Biol.* **2011**, *8*, 207-215.
- (15) Hutchinson, E. C.; Fodor, E. Transport of the Influenza Virus Genome From Nucleus to Nucleus. *Viruses* **2013**, *5*, 2424-2446.
- (16) Plotch, S. J.; Bouloy, M.; Ulmanen, I.; Krug, R. M. A Unique Cap(m7GpppXm)-Dependent Influenza Virion Endonuclease Cleaves Capped RNAs to Generate the Primers that Initiate Viral RNA Transcription. *Cell* **1981**, *23*, 847-858.
- (17) Dias, A.; Bouvier, D.; Crepin, T.; McCarthy, A. A.; Hart, D. J.; Baudin, F.; Cusack, S.; Ruigrok, R. W. The Cap-Snatching Endonuclease of Influenza Virus Polymerase Resides in the PA Subunit. *Nature* **2009**, *458*, 914-918.
- (18) Yuan, P. W.; Bartlam, M.; Lou, Z. Y.; Chen, S. D.; Zhou, J.; He, X. J.; Lv, Z. Y.; Ge, R. W.; Li, X. M.; Deng, T.; Fodor, E.; Rao, Z. H.; Liu, Y. F. Crystal Structure of an Avian Influenza Polymerase PA(N) Reveals an Endonuclease Active Site. *Nature* **2009**, *458*, 909-913.
- (19) Guilligay, D.; Tarendeau, F.; Resa-Infante, P.; Coloma, R.; Crepin, T.; Sehr, P.; Lewis, J.; Ruigrok, R. W. H.; Ortin, J.; Hart, D. J.; Cusack, S. The Structural Basis for Cap Binding by Influenza Virus Polymerase Subunit PB2. *Nat. Struct. Mol. Biol.* **2008**, *15*, 500-506.
- (20) Crepin, T.; Dias, A.; Palencia, A.; Swale, C.; Cusack, S.; Ruigrok, R. W. H. Mutational and Metal Binding Analysis of the Endonuclease Domain of the Influenza Virus Polymerase PA Subunit. *J. Virol.* **2010**, *84*, 9096-9104.
- (21) Rao, P.; Yuan, W. M.; Krug, R. M. Crucial Role of CA Cleavage Sites in the Cap-Snatching Mechanism for Initiating Viral mRNA Synthesis. *Embo J.* **2003**, *22*, 1188-1198.
- (22) Credille, C. V.; Dick, B. L.; Morrison, C. N.; Stokes, R. W.; Adamek, R. N.; Wu, N. C.; Wilson, I. A.; Cohen, S. M. Structure-Activity Relationships in Metal-Binding Pharmacophores for Influenza Endonuclease. *J. Med. Chem.* **2018**, *61*, 10206-10217.
- (23) Bauman, B. M.; Slavish, P. J.; DuBois, R. M.; Boyd, V. A.; White, S. W.; Webb, T. R. Identification of Influenza Endonuclease Inhibitors Using a Novel Fluorescence Polarization Assay. *ACS Chem Biol* **2012**, *7*, 526-534.
- (24) Ju, H.; Zhang, J.; Huang, B. S.; Kang, D. W.; Huang, B.; Liu, X. Y.; Zhan, P. Inhibitors of Influenza Virus Polymerase Acidic (PA) Endonuclease: Contemporary Developments and Perspectives. *J. Med. Chem.* **2017**, *60*, 3533-3551.
- (25) Rogolino, D.; Carcelli, M.; Sechi, M.; Neamati, N. Viral Enzymes Containing Magnesium: Metal Binding as a Successful Strategy in Drug Design. *Coord. Chem. Rev.* **2012**, *256*, 3063-3086.
- (26) Bauman, J. D.; Patel, D.; Baker, S. F.; Vijayan, R. S. K.; Xiang, A.; Parhi, A. K.; Martinez-Sobrido, L.; LaVoie, E. J.; Das, K.; Arnold, E. Crystallographic Fragment Screening and Structure-Based Optimization Yields a New Class of Influenza Endonuclease Inhibitors. *ACS Chem Biol* **2013**, *8*, 2501-2508.
- (27) Credille, C. V.; Chen, Y.; Cohen, S. M. Fragment-Based Identification of Influenza Endonuclease Inhibitors. *J. Med. Chem.* **2016**, *59*, 6444-6454.

- (28) Kowalinski, E.; Zubieta, C.; Wolkerstorfer, A.; Szolar, O. H. J.; Ruigrok, R. W.; Cusack, S. Structural Analysis of Specific Metal Chelating Inhibitor Binding to the Endonuclease Domain of Influenza pH1N1 (2009) Polymerase. *PLoS Pathog.* **2012**, *8*, e1002831.
- (29) Stevaert, A.; Nurra, S.; Pala, N.; Carcelli, M.; Rogolino, D.; Shepard, C.; Domaal, R. A.; Kim, B.; Alfonso-Prieto, M.; Marras, S. A. E.; Sechi, M.; Naesens, L. An Integrated Biological Approach to Guide the Development of Metal-Chelating Inhibitors of Influenza Virus PA Endonuclease. *Mol. Pharm.* **2015**, *87*, 323-337.
- (30) Omoto, S.; Speranzini, V.; Hashimoto, T.; Noshi, T.; Yamaguchi, H.; Kawai, M.; Kawaguchi, K.; Uehara, T.; Shishido, T.; Naito, A.; Cusack, S. Characterization of Influenza Virus Variants Induced by Treatment with the Endonuclease Inhibitor Baloxavir Marboxil. *Sci. Rep.* **2018**, *8*, 9633.
- (31) Beylkin, D.; Kumar, G.; Zhou, W.; Park, J.; Jeevan, T.; Lagiseti, C.; Harfoot, R.; Webby, R. J.; White, S. W.; Webb, T. R. Protein-Structure Assisted Optimization of 4,5-Dihydropyrimidine-6-Carboxamide Inhibitors of Influenza Virus Endonuclease. *Sci. Rep.* **2017**, *7*.
- (32) Simeonov, A. Recent Developments in the Use of Differential Scanning Fluorometry in Protein and Small Molecule Discovery and Characterization. *Expert Opin. Drug Discov.* **2013**, *8*, 1071-1082.
- (33) Zhang, R.; Monsma, F. Fluorescence-Based Thermal Shift Assays. *Curr. Opin. Drug Discov. Devel.* **2010**, *13*, 389-402.
- (34) Matulis, D.; Kranz, J. K.; Salemme, F. R.; Todd, M. J. Thermodynamic Stability of Carbonic Anhydrase: Measurements of Binding Affinity and Stoichiometry Using ThermoFluor. *Biochemistry* **2005**, *44*, 5258-5266.
- (35) Bergsdorf, C.; Ottl, J. Affinity-Based Screening Techniques: Their Impact and Benefit to Increase the Number of High Quality Leads. *Expert Opin. Drug Discov.* **2010**, *5*, 1095-1107.
- (36) Sagong, H. Y.; Bauman, J. D.; Patel, D.; Das, K.; Arnold, E.; LaVoie, E. J. Phenyl Substituted 4-Hydroxypyridazin-3(2H)-ones and 5-Hydroxypyrimidin-4(3H)-ones: Inhibitors of Influenza A Endonuclease. *J. Med. Chem.* **2014**, *57*, 8086-8098.
- (37) Dick, B. L.; Patel, A.; McCammon, J. A.; Cohen, S. M. Effect of Donor Atom Identity on Metal-Binding Pharmacophore Coordination. *J. Biol. Inorg. Chem.* **2017**, *22*, 605-613.
- (38) DuBois, R. M.; Slavish, P. J.; Baughman, B. M.; Yun, M. K.; Bao, J.; Webby, R. J.; Webb, T. R.; White, S. W. Structural and Biochemical Basis for Development of Influenza Virus Inhibitors Targeting the PA Endonuclease. *PLoS Pathog.* **2012**, *8*, e1002830.
- (39) Jones, J. C.; Marathe, B. M.; Lerner, C.; Kreis, L.; Gasser, R.; Pascua, P. N. Q.; Najera, I.; Govorkova, E. A. A Novel Endonuclease Inhibitor Exhibits Broad-Spectrum Anti-Influenza Virus Activity In Vitro. *Antimicrob. Agents Chemother.* **2016**, *60*, 5504-5514.

Table of Contents Entry

